Use of an insulating mask for controlling anisotropy in multilayer electrospun scaffolds for tissue engineering†

N. William Garrigues,[ab] Dianne Little,[a] Christopher J. O'Conor[a] and Farshid Guilak*[ab]

Received 13th June 2010, Accepted 17th August 2010
DOI: 10.1039/c0jm01880e

Tissue engineering of various musculoskeletal or cardiovascular tissues requires scaffolds with controllable mechanical anisotropy. However, native tissues also exhibit significant inhomogeneity in their mechanical properties, and the principal axes of anisotropy may vary with site or depth from the tissue surface. Thus, techniques to produce multilayered biomaterial scaffolds with controllable anisotropy may provide improved biomimetic properties for functional tissue replacements. In this study, poly(ε-caprolactone) scaffolds were electrospun onto a collecting electrode that was partially covered by rectangular or square shaped insulating masks. The use of a rectangular mask resulted in aligned scaffolds that were significantly stiffer in tension in the axial direction than the transverse direction at 0 strain (22.9 ± 1.3 MPa axial, 16.1 ± 0.9 MPa transverse), and at 0.1 strain (4.8 ± 0.3 MPa axial, 3.5 ± 0.2 MPa transverse). The unaligned scaffolds, produced using a square mask, did not show this anisotropy, with similar stiffness in the axial and transverse directions at 0 strain (19.7 ± 1.4 MPa axial, 20.8 ± 1.3 MPa transverse) and 0.1 strain (4.4 ± 0.2 MPa axial, 4.6 ± 0.3 MPa, transverse). Aligned scaffolds also induced alignment of adipose stem cells near the expected axis on aligned scaffolds (0.015 ± 0.056 rad), while on the unaligned scaffolds, their orientation showed more variation and was not along the expected axis (1.005 ± 0.225 rad). This method provides a novel means of creating multilayered electrospun scaffolds with controlled anisotropy for each layer, potentially providing a means to mimic the complex mechanical properties of various native tissues.

Introduction

Tissue engineering seeks to apply combinations of cells, biomaterial scaffolds, and bioactive molecules to enhance the repair or regeneration of injured or diseases tissues. Despite many rapid advances, challenges still remain with respect to the development of functional replacements for tissues that primarily serve a biomechanical role, such as musculoskeletal tissues.[1] In this regard, the mechanical properties of the biomaterial scaffold can play an important role in the success of the engineered tissue not only by providing structural support during early phases of tissue regeneration, but also by influencing cell alignment, tissue growth, and differentiation through physical interactions with cells.[2] In particular, recent studies suggest that the size and orientation of nanoscale structures within a biomaterial scaffold may have a significant influence on cell behavior and alignment.[3–9] Therefore, the ability to define scaffold architecture at multiple length scales may provide novel means of enhancing cell-based tissue engineering.

Electrospun scaffolds have shown promise in the engineering of many tissues, including cartilage, meniscus, tendon, bone, fat, heart valve, intervertebral disc, and muscle.[5–7,10–16] The scaffolds can be engineered to have controllable and versatile properties, such as hollow fibers containing cells, controllable drug release, or chemical functionalization.[17–20] Electrospun scaffolds can be produced using nearly any polymer, have controllable fiber diameter, and support cell attachment and proliferation.[21–24] Further, the nanoscale fiber size prompts a diminished foreign body response *in vivo*, and has advantageous effects on the phenotype of chondrocytes cultured on electrospun scaffolds.[9,25–27]

Because electrospinning of nanofibers onto a collecting plate produces a randomly aligned scaffold, efforts to apply electrospun scaffolds to the mechanical requirements of various engineered tissues have focused on the introduction of mechanical anisotropy (mechanical properties that vary with direction) into the scaffold.[8,16,28–30] In addition to the stiffness of the scaffold, the alignment of nanofibers has even been shown to affect cell alignment and phenotype, as well as the structure of the deposited extracellular matrix.[3–5,8,28,31–33] Interest in anisotropic scaffolds is broad, including anisotropic woven scaffolds,[34] and methods to align electrospun fibers.[11] Various techniques to create anisotropy have been used and include moving the collector electrode to physically pull the fibers into alignment, typically by collecting fibers on a rapidly spinning mandrel.[8,29,30,35,36] This technique is successful in producing highly anisotropic scaffolds for tissue engineering, but does not directly allow the formation of multilayered scaffolds with differing anisotropy; rather, individual aligned layers must be removed and combined, or cultured to form a composite using deposited extracellular matrix *in vitro*.[37] Another method to align fibers involves shaping the electrodes and interspersing insulators

[a]*Orthopaedic Research Laboratories, Department of Orthopaedic Surgery, Duke University Medical Center, 375 MSRB, Box 3093, Durham, North Carolina, 27710, USA. E-mail: guilak@duke.edu; Fax: +(919) 681-8490; Tel: +(919) 684-2521*
[b]*Department of Biomedical Engineering, Duke University, Durham, NC, 27708, USA*

† This paper is part of a joint *Journal of Materials Chemistry* and *Soft Matter* themed issue on Tissue Engineering. Guest editors: Molly Stevens and Ali Khademhosseini.

to collect the fibers that align across the insulating gap.[38–40] This method produces highly aligned fibers but is not suitable for making thick scaffolds that are often required for tissue engineering. Further, current methods for creating anisotropy in electrospun scaffolds are unable to imitate the unique properties of individual layers of human tissue in the construction of each layer of the scaffold. To better approximate the nano- and micro-scale architecture of different tissues, it is necessary to create scaffolds with controlled mechanical anisotropy, so that the properties of each layer can be independently controlled based on the type of tissue being grown.

In this study, we developed a method for creating a multilayered electrospun scaffold, with each layer having its own preferred fiber direction, without requiring lamination for consolidation of the different layers. We used rectangular and square insulating masks to control the geometry of the electric field, which controls the alignment of the deposited fibers and generates mechanical anisotropy in the resulting scaffold. We analyzed fiber alignment, the tensile mechanical properties in two orthogonal directions, and alignment of adipose stem cells when cultured on the scaffolds.

Materials and methods

Electrospinning

Poly(ε-caprolactone) (PCL) ($M_n = 42{,}500$, $M_w = 65{,}000$) (Sigma Aldrich, St. Louis, MO) was dissolved at 15% (w/v) in a solvent of 70% (v/v) dichloromethane (Sigma Aldrich, St. Louis, MO) and 30% ethanol at room temperature overnight. The PCL solution was pumped with a syringe pump (Cole-Parmer Instrument Co., 74900-00, Vernon Hills, IL) through a blunt-tip 25 gauge needle with a round focusing cage (3 cm diameter, 4 mm above end of needle tip) at 4 ml/h across a 14 cm gap with 20 kV applied (Gamma High Voltage Research, Ormond Beach, FL) for 7 min. The pump was turned off at this time and the system was given 4 min to stop electrospinning due to the residual pressure in the pump. The collecting electrode was a 12.5 cm square flat copper plate, with a polysiloxane rubber insulating mask placed on top (Fig. 1). The rubber masks were 13.2 cm square, 0.16 cm thick, with a 25 cm^2 opening cut in the center. One mask had a square aperture (5 cm × 5 cm) (producing what we have termed "unaligned scaffolds"), and the other had a rectangular aperture (10 cm × 2.5 cm) (producing what we have termed "aligned scaffolds"), such that the two masks have exposed surfaces that are equal in area.

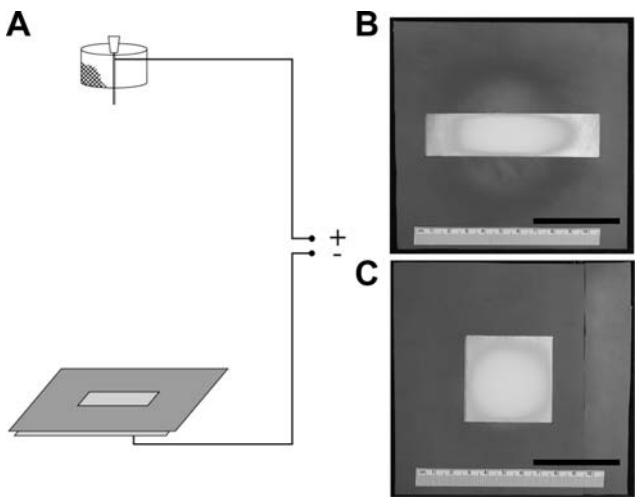

Fig. 1 (A) Electrospinning apparatus. The copper collector electrode is covered by a rubber insulating mask with a 25 cm^2 aperture. (B, C) Scaffolds on collector electrode with insulating masks *in situ*. (B) Rectangular mask and scaffold. Note the small amount of fibers collected on the mask. (C) Square mask and scaffold. Scale bar = 5 cm.

Mechanical testing

Scaffolds were tested in tension in both the axial (parallel with the long axis of the rectangular mask or a given side of the square mask) and transverse directions (orthogonal to the axial direction). Scaffolds were prepared for mechanical testing by pre-wetting with PBS (pH 7.4). Because PCL is hydrophobic, samples were initially submerged in ethanol, and then graduated concentrations of ethanol/PBS until the samples were left in PBS overnight. Samples were cut with a dog-bone shaped die that had a central section 1 mm wide and 10 mm long. Tensile tests were performed in a universal testing machine (Bose EnduraTEC SmartTest, Eden Prairie, MN) with a 2 gf tare load at 0.1% strain/s, with strain data gathered using a digital camera (Sony XCD-X700, Tokyo, Japan) every 1 s. Thickness was calculated using an adjacent section of the scaffold and the camera, using digital callipers in Vision Builder (National Instruments, Austin, TX). True stress was determined by dividing the force by the cross-sectional area of the specimen, corrected for narrowing in width (Fig. 3). All other data and calculations employed engineering stress and infinitesimal strain. A minimum of 11–13 scaffolds were tested from each group in each direction, for a total of n = 47 scaffolds.

Fiber alignment measurement

The fast Fourier Transform (FFT) was used to analyze fiber orientation in the scaffolds, based on a modification of the technique reported previously.[41–43] One to three 6 mm punches were taken from each scaffold, at least 0.5 cm away from the edges. Using a scanning electron microscope (SEM) (FEI XL30 ESEM, Hillsboro, OR), at least 3 images of random, non-overlapping locations away from the edge were taken of each punch, yielding 4–9 images each scaffold (n = 8-9 specimens per group) at 1000x magnification. Scaffolds were sputter-coated with gold and palladium (Desk IV, Denton Vacuum, Moorestown, NJ) before imaging. Image analysis was performed in MATLAB (MathWorks, Natick, MA) as follows: Images were cropped to a square, thresholded using Otsu's method, and then masked with a radial gradient to gray before a 2D fast Fourier Transform was applied. Pixel intensities were summed along the radius of the power spectrum, with bilinear interpolation, at intervals of 1°, then normalized by area and recentered on 0. Peaks due to pixel edges were automatically removed by replacing the data from the 5° on either side of 0° with a linear interpolation between the averages of the next 5° on either side. This was repeated at 90°. Profiles from each image of the same punch were averaged, and then the profiles from each punch of the same

scaffold were averaged to get an overall profile for each scaffold. Data were normalized to show actual angle of alignment relative to the expected angle of alignment.

The data was analyzed in two ways. First, the average height of the profile for the 15° on either side of the expected orientation was designated the Fiber Alignment Index, with higher values meaning that the fibers within a scaffold were more aligned in the expected direction. Second, the profile from each scaffold was fit using MATLAB to a sinusoid of the form $y = A*\sin(2x + \pi/2 + B)$ where A and B were the amplitude and phase shift, respectively, to examine the degree and direction of alignment without constraining analysis to the expected direction.

Multilayer scaffolds

Multilayer scaffolds consisted of more than one layer of scaffold being produced using the rectangular mask in the same way as above, with each layer having a different mask orientation from the preceding layer. After 7 min of electrospinning to produce the first layer, the insulating mask was rotated 90° relative to the collecting electrode and attached scaffold, without stopping the electrospinning process. Scaffolds were produced with 2 layers and evaluated for fiber alignment as above.

Cell alignment

Single layer scaffolds were cut to a round shape with a small straight edge in the expected alignment direction, then treated with 4 M NaOH for 18 h to increase hydrophilicity before rinsing and sterilizing in ethanol with UV light. The scaffolds were then soaked with ethanol, then PBS, then incubated with fetal bovine serum (Zen-Bio, Research Triangle Park, NC) overnight at 37 °C. These prepared scaffolds were then seeded with passage 5 adipose stem cells at 200,000 cells/cm^2.[44,45] The constructs were cultured with expansion medium consisting of Dulbecco's Modified Eagle's Medium: Nutrient Mixture F-12 (Gibco, Grand Island, NY), 10% fetal bovine serum (Zen-Bio, Research Triangle Park, NC), 1% penicillin-streptomycin (Invitrogen, Carlsbad, CA), 5 ng/ml recombinant human epidermal growth factor (Roche Diagnostics, Indianapolis, IN), 1 ng/ml recombinant human basic fibroblastic growth factor (Roche Diagnostics, Indianapolis, IN), and 0.25 ng/ml transforming growth factor-β1 (R&D Systems, Minneapolis, MN) for 4 days before being stained with Syto 13 nuclear stain (Invitrogen, Carlsbad, CA) and imaged on a 510 confocal laser scanning microscope (Carl Zeiss MicroImaging, Thornwood, NY). Images were analyzed in MATLAB by fitting an ellipse to each nucleus and calculating the orientation of the major axis relative to the expected angle.

Statistical analysis

All data were expressed as mean ± standard error of the mean. Rayleigh's test of uniformity and all other statistics for phase shift data were performed using the Circular Statistics Toolbox for Matlab. The variances of phase shift were compared using an F-test. Mechanical data were analyzed with a 2 factor ANOVA, while fiber alignment data were analyzed with a one-way ANOVA. Fisher's post-hoc test was used for all ANOVA data. Significance was reported at the 95% confidence interval ($\alpha = 0.05$).

Results

Gross morphology of electrospun PCL scaffolds

The scaffolds produced by the masked electrospinning process were affected by the shape of the aperture in the insulating mask used for their production (Fig. 1). The square mask produced circular scaffolds with edges just touching all four sides of the mask, while the rectangular mask produced scaffolds that were elliptical, touched only the two long sides of the mask, and had only a few fibers that were deposited directly on the mask. The scaffolds were otherwise similar in gross morphology and appeared similar by scanning electron microscope (Fig. 2). The mean thickness of the scaffolds used for mechanical testing was 0.35 ± 0.02 mm for the aligned scaffolds and 0.30 ± 0.02 mm for the unaligned scaffolds ($p = 0.11$).

Tensile testing

Aligned scaffolds (produced using a rectangular mask) displayed distinct mechanical anisotropy, while the unaligned scaffolds (produced using a square mask) did not (Fig. 4). The aligned scaffolds were stiffer in the axial direction than the transverse direction at 0 strain (22.9 ± 1.3 MPa axial, 16.1 ± 0.9 MPa transverse; $p < 0.0005$), and at 0.1 strain (4.8 ± 0.3 MPa axial, 3.5 ± 0.2 MPa transverse; $p < 0.001$) ($n = 12, 13$). The unaligned scaffolds did not show this difference, with similar stiffness in the

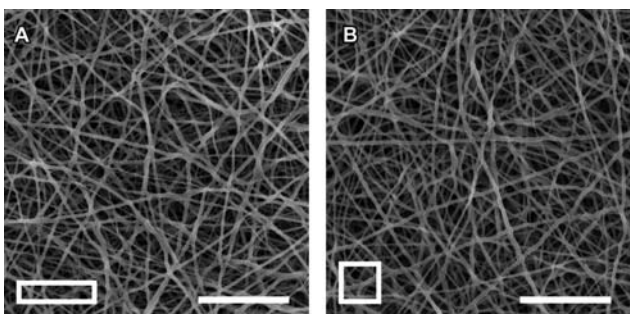

Fig. 2 Scanning electron micrographs of scaffolds produced using (A) rectangular mask (aligned scaffold) and (B) square mask (unaligned scaffold). Expected axis is horizontal. (1000× magnification. Scale bar = 50 μm.)

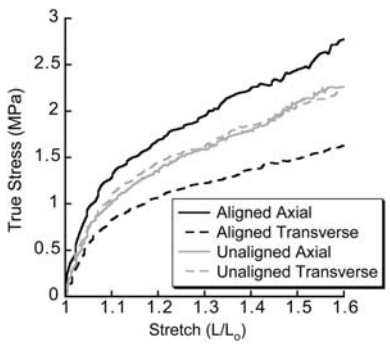

Fig. 3 True stress v. stretch curves for representative scaffolds. Note that the axial and transverse unaligned curves are almost superimposed and the aligned scaffolds show higher stress and stiffness in the axial direction compared to the transverse direction.

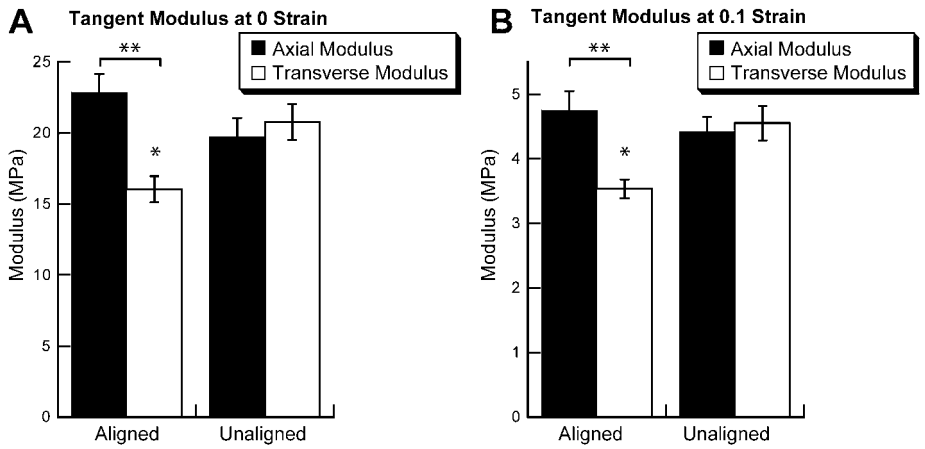

Fig. 4 Tangent moduli at (A) 0 strain and (B) 0.1 strain for scaffolds tested in axial and transverse directions. Aligned scaffolds are stiffer in the axial direction. (** $p < 0.0005$ for 0 strain, $p < 0.001$ for 0.1 strain.) Unaligned scaffolds, axial and transverse directions not different: $p = 0.54$ for 0 strain, $p = 0.70$ for 0.1 strain. * Denotes that aligned transverse modulus is different from all other groups, $p < 0.05$. (Mean ± SEM.)

axial and transverse directions at 0 strain (19.7 ± 1.4 MPa axial, 20.8 ± 1.3 MPa transverse; $p = 0.54$) and 0.1 strain (4.4 ± 0.2 MPa axial, 4.6 ± 0.3 MPa, transverse; $p = 0.70$) ($n = 11$ per group). The scaffolds displayed a strain-softening or yielding response characterized by linear regions at 0 strain, decaying to a lower modulus linear region at high strain (Fig. 3).

Fiber alignment

The aligned scaffolds exhibited a higher Fiber Alignment Index (0.97 ± 0.16) than the unaligned scaffolds, where it approximated 0 (0.11 ± 0.15) ($p < 0.0005$) (Fig. 5A,B). Aligned scaffolds showed a trend towards exhibiting better fits to a sine curve ($R^2 = 0.52 \pm 0.09$) than the unaligned scaffolds ($R^2 = 0.30 \pm 0.09$) ($p = 0.076$). Aligned scaffolds also showed greater amplitude (0.73 ± 0.15) than the unaligned scaffolds (0.42 ± 0.12) ($p = 0.087$) (Fig. 5C), and smaller phase shifts (0.26 ± 0.16 rad *vs.* 1.08 ± 0.42 rad for unaligned) with a much smaller range ($p < 0.05$) and higher mean vector magnitude (0.88 *vs.* 0.29 for unaligned) (Fig. 5D). The phase shift values fit a von Mises distribution for the aligned scaffolds ($p < 0.0005$), but not for the unaligned scaffolds ($p = 0.53$).

Multilayer fiber alignment

Multilayered scaffolds showed more alignment in the top layer (Fiber Alignment Index: 1.98 ± 0.16) than single-layered aligned scaffolds ($p < 0.0001$) (Fig. 5B). The sine curves showed higher amplitude (1.69 ± 0.07) than the single layered aligned scaffolds (0.73 ± 0.15, $p < 0.0001$). The top layer of the multilayered scaffolds showed phase shift of 0.01 ± 0.13 with a mean vector magnitude of 0.96, and conformed to a von Mises distribution ($p < 0.001$).

Cell alignment

Nearly all of the cells cultured on the single layer scaffolds had an elliptical nucleus (scaffolds had 92.7 ± 0.5% of nuclei with an aspect ratio greater than 1.5), and most scaffolds had a principal direction of cell alignment, with more cells being oriented in one direction (Fig. 6). The aligned scaffolds showed a greater degree of cell alignment than the unaligned scaffolds, with more cells oriented close to the principal direction of alignment (standard deviation 0.288 ± 0.018 rad, compared to 0.496 ± 0.029, $p < 0.0005$), and a larger mean vector magnitude (0.83 ± 0.02, compared to 0.50 ± 0.06, $p < 0.0005$). The cell orientation in the aligned scaffolds was close to the expected axis (0.015 ± 0.056 rad), while in the unaligned scaffolds, it was not (1.005 ± 0.225 rad) (different at $p < 0.05$). Additionally, the principal direction of alignment for each scaffold varied less for the aligned scaffolds than the unaligned scaffolds ($p < 0.01$).

Discussion

Our findings present a novel method for creating a multilayered electrospun scaffold, with each layer having its own preferred direction of fiber alignment in order to mimic human tissues. The results of this study demonstrate that macroscopic shaped insulating masks can be used to create aligned multilayered scaffolds with each layer having anisotropy in a different direction. Mechanical anisotropy with approximately 30–40% difference in stiffness is associated with increased fiber alignment, and alignment of adipose stem cells cultured on the surface.

Scaffolds produced using a rectangular insulating mask showed a significant difference of approximately 35% in tensile moduli in two orthogonal directions. Such anisotropy primarily has been achieved in the past using rapidly spinning mandrels, physically pulling the fibers into alignment.[8,29,30,35,36] This spinning mandrel method can produce much higher levels of anisotropy, which can exceed modulus ratios of 10 : 1 at high spinning rates.[5] The approach described here introduces lower levels of anisotropy (approximately 35% difference in moduli), but which are similar to those observed in native tissues. For example, native articular cartilage possesses a similar level of anisotropy as the scaffolds produced with our method described here. The cartilage of the humeral head has a tensile modulus of 7.8 MPa in the direction of the split lines, and 5.9 MPa perpendicular to them. This difference of 32–35% stiffer in the split line direction is maintained throughout the thickness of the cartilage

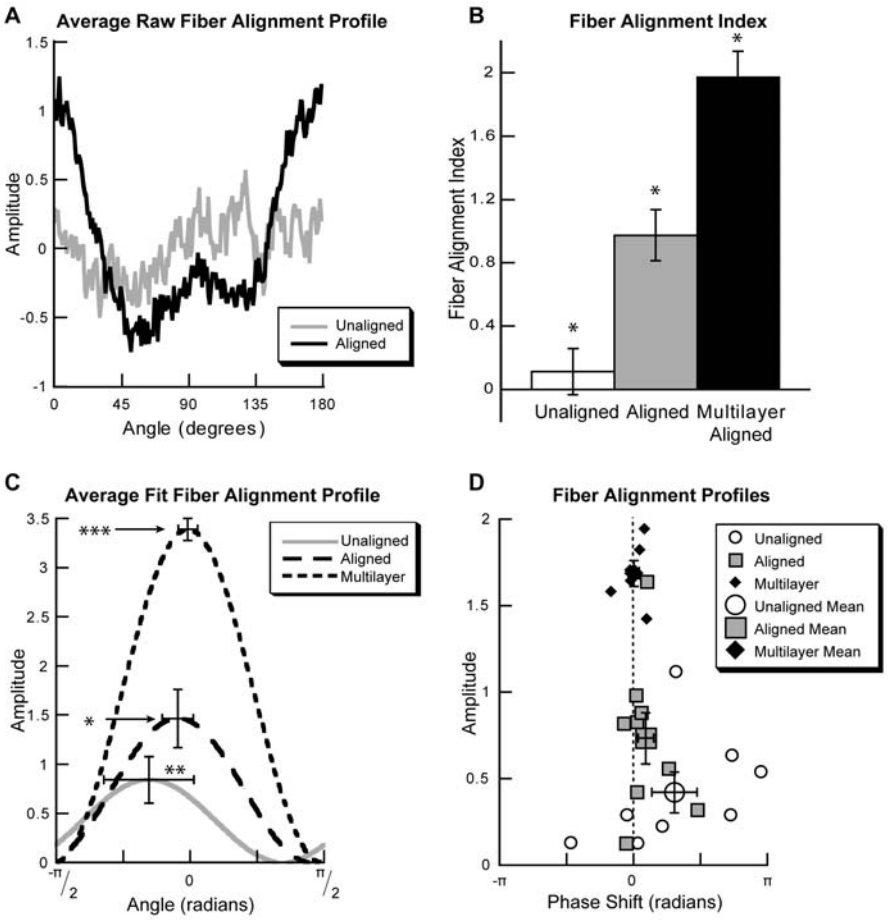

Fig. 5 Fiber alignment. (A) Average fast Fourier Transform profiles of aligned and unaligned scaffolds (n = 8-9 scaffolds per group). (B) Fiber Alignment Index for unaligned, aligned, and multilayer aligned scaffolds. All groups are different ($p < 0.0005$). (C) Sine curve constructed from mean fit parameters, showing SEM of amplitude and phase shift. * amplitude of aligned greater than amplitude of unaligned ($p = 0.087$). *** amplitude of multilayer aligned greater than other groups ($p < 0.0001$). ** variance of unaligned phase shift greater than other groups ($p < 0.05$). (D) Fiber alignment profiles for each unaligned, aligned and multilayer aligned scaffold, and means for each group. Note distribution of aligned and multilayer aligned scaffolds near 0 phase shift and distribution of unaligned scaffold over a much greater phase shift range. Dotted line denotes the expected angle. All error bars represent SEM.

and increased to 63% in the surface zone at 0.16 strain.[46] The aligned scaffolds presented here are 42% stiffer in the axial direction at 0 strain and 34% stiffer at 0.1 strain, which is similar to published values for cartilage.[47] Though the level of anisotropy of the produced scaffolds is lower than in those made with a spinning mandrel, the technique described here achieved a comparable level of anisotropy to cartilage, while allowing multiple directions of alignment in subsequent layers. Increasing the aspect ratio or otherwise changing the shape of the insulating mask could provide further anisotropy in the resulting scaffolds. Furthermore, the process described may be particularly useful for the engineering of tissues that display inhomogeneity in the mechanical anisotropy with different layers, such as the anulus fibrosus, which has successive layers with principal orientations 30° on either side of the spine's transverse axis.[37]

The introduction of anisotropy to the scaffolds using the described technique occurs through the increased alignment of fibers in a preferred direction, similar to what has been reported with other anisotropic electrospinning methods.[5,41–43] This directionality is relatively subtle and not noticeable by simple observation (Fig. 2). The Fiber Alignment Index reported here provides a means of simplifying the FFT data into a single quantity (Fig. 5B). A positive value of the index indicates that a group of scaffolds shows alignment along the expected direction, as in the aligned scaffolds (0.97 ± 0.16). Because it represents the magnitude of the profile in the preferred direction after the profile has been centered on 0, a group of scaffolds without a preferred direction has an expected value of 0, as we see with the unaligned scaffolds (0.11 ± 0.15). However, the profiles from unaligned scaffolds often display some degree of periodicity, and averaging them together can obscure this. Therefore, we further investigated how these scaffolds appear to display fiber alignment when examined individually.

Amplitude and phase shift values are more instructive than the Fiber Alignment Index in understanding the fiber alignment in individual electrospun scaffolds (Fig. 5C, 5D). Though the amplitude was higher in the aligned scaffolds than in the unaligned scaffolds, as expected, the amplitude in the unaligned scaffolds

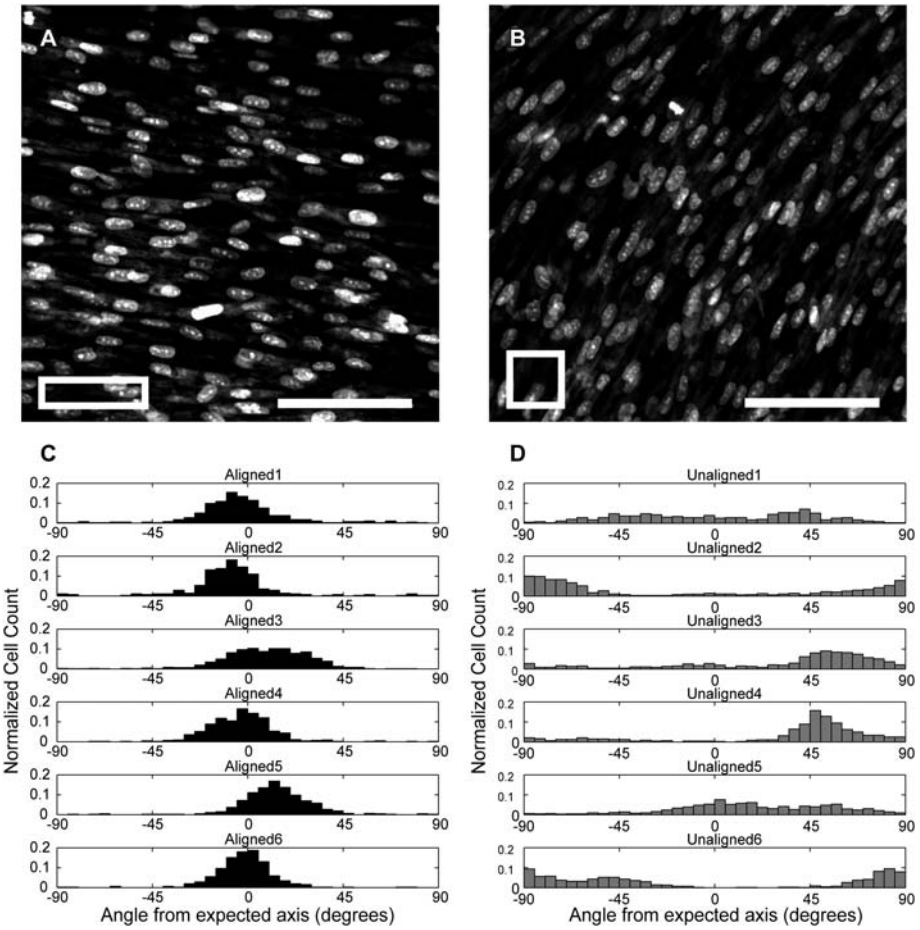

Fig. 6 Adipose stem cells (nuclei stained with Syto 13) cultured on (A) aligned and (B) unaligned scaffolds. Expected axis is horizontal. Scale bar = 100 μm. (C, D) Cell orientation histograms from 6 (C) aligned and (D) unaligned scaffolds.

was not zero, showing that the unaligned scaffolds show some degree of periodicity in their profiles. The phase shifts, which give the preferred alignment angle, were grouped near the expected alignment value of 0 for the aligned scaffolds, but were distributed uniformly across the full possible range in the unaligned scaffolds (Fig. 5D). Examining the mean for each type of scaffold demonstrates that the profiles of the unaligned scaffolds are not flat, but do show a large variation in phase shift. This variation in phase shifts in the unaligned scaffolds results in a flat line when scaffolds from an entire group are averaged together (Fig. 5A). On the other hand, the aligned scaffolds have a much narrower range of phase shifts, causing the averaging of an entire group to preserve the periodic shape. This explains why the Fiber Alignment Index is near 0 for the unaligned scaffolds, but each scaffold does show periodicity. This analysis provides insights into how fibers are aligned in electrospun scaffolds. We have demonstrated that electrospun scaffolds exhibiting mechanical isotropy tend to show surface fiber alignment in an arbitrary direction. The fiber orientation in the aligned scaffold was consistent with the alignment of the long sides of the rectangular insulating mask.

Fiber alignment occurs based on the orientation of attractive forces generated by the shaped collector electrode. Previous work has shown that fibers collected on a thin electrode surrounded by insulators show orientation along the axis of the electrode.[38] Our results indicate that this effect persists when the elongated electrode is widened from less than 1 mm to 2.5 cm. The technique described here allows this alignment due to an elongated electrode to be harnessed for use in a multilayered scaffold.

The multilayer scaffolds exhibited more pronounced alignment in the top layer than the single-layer scaffolds. Because the bottom layer was manufactured in an identical way to the single layered scaffolds, this data indicates that anisotropy can be imparted by the rectangular mask even if the collector electrode is partially covered by a previous layer. Further, this partial coverage of the collector electrode is most likely the cause of the increased fiber alignment in the top layer. As the second layer is deposited, the central area is concealed by the previous layer, forming an insulator between two exposed electrodes. An insulator between electrodes has been shown to align the fibers between the electrodes.[39,40]

The differences between aligned and unaligned scaffolds were also observed in the cell alignment studies (Fig. 6). Cells seeded on the scaffold surfaces exhibited local regions of alignment, as measured by the principal direction of the nuclei, in both aligned and unaligned scaffolds. Aligned scaffolds showed a significant mean cell orientation in the principal axis of alignment of the scaffold, whereas unaligned scaffolds showed a smaller but nonzero level of cell alignment in random directions.

In summary, this study provides proof-of-concept of a novel method for creating multilayered anisotropic electrospun scaffolds for tissue engineering that may meet the mechanical needs of tissue as well as influence the alignment of cultured cells. The use of a rectangular insulating mask induces a preferential alignment direction into scaffolds. Cells seeded onto these scaffolds also showed preferential alignment along the expected axis of alignment of the insulating mask. Further studies are needed to examine the growth and differentiation of cells on these scaffolds as well as the influence of alignment on the long-term mechanical properties of cell-seeded constructs.

Acknowledgements

Supported in part by NIH grants AR48852, AG15768, AR48182, and AR50245, GM008719, the Duke Translational Research Institute (RR24128), and by an unrestricted fellowship grant from Synthes, Inc. The authors would like to thank Jason Klein, Ian Gao and Frank Moutos for their contributions to the anisotropic electrospinning development.

References

1 D. L. Butler, S. A. Goldstein and F. Guilak, *J. Biomech. Eng.*, 2000, **122**, 570–575.
2 F. Guilak, D. M. Cohen, B. T. Estes, J. M. Gimble, W. Liedtke and C. S. Chen, *Cell Stem Cell*, 2009, **5**, 17–26.
3 S. Y. Chew, R. Mi, A. Hoke and K. W. Leong, *Biomaterials*, 2008, **29**, 653–661.
4 E. K. F. Yim, R. M. Reano, S. W. Pang, A. F. Yee, C. S. Chen and K. W. Leong, *Biomaterials*, 2005, **26**, 5405–5413.
5 W. J. Li, R. L. Mauck, J. A. Cooper, X. Yuan and R. S. Tuan, *J. Biomech.*, 2007, **40**, 1686–1693.
6 W. J. Li, R. Tuli, X. Huang, P. Laquerriere and R. S. Tuan, *Biomaterials*, 2005, **26**, 5158–5166.
7 J. S. Choi, S. J. Lee, G. J. Christ, A. Atala and J. J. Yoo, *Biomaterials*, 2008, **29**, 2899–2906.
8 B. M. Baker and R. L. Mauck, *Biomaterials*, 2007, **28**, 1967–1977.
9 W. J. Li, Y. J. Jiang and R. S. Tuan, *Tissue Eng.*, 2006, **12**, 1775–1785.
10 J. A. Stella, J. Liao, Y. Hong, W. David Merryman, W. R. Wagner and M. S. Sacks, *Biomaterials*, 2008, **29**, 3228–3236.
11 R. L. Mauck, B. M. Baker, N. L. Nerurkar, J. A. Burdick, W. J. Li, R. S. Tuan and D. M. Elliott, *Tissue Eng., Part B: Rev.*, 2009, **15**, 171–193.
12 S. D. McCullen, Y. Zhu, S. H. Bernacki, R. J. Narayan, B. Pourdeyhimi, R. E. Gorga and E. G. Loboa, *Biomed. Mater.*, 2009, **4**, 35002.
13 S. G. Kumbar, R. James, S. P. Nukavarapu and C. T. Laurencin, *Biomed. Mater.*, 2008, **3**, 034002.
14 E. M. Christenson, K. S. Anseth, J. J. J. P. v. d. Beucken, C. K. Chan, B. Ercan, J. A. Jansen, C. T. Laurencin, W.-J. Li, R. Murugan, L. S. Nair, S. Ramakrishna, R. S. Tuan, T. J. Webster and A. G. Mikos, *J. Orthop. Res.*, 2007, **25**, 11–22.
15 Q. P. Pham, U. Sharma and A. G. Mikos, *Tissue Eng.*, 2006, **12**, 1197–1211.
16 T. Courtney, M. S. Sacks, J. Stankus, J. Guan and W. R. Wagner, *Biomaterials*, 2006, **27**, 3631–3638.
17 S. N. Jayasinghe and A. Townsend-Nicholson, *Lab Chip*, 2006, **6**, 1086–1090.
18 K. J. Shields, M. J. Beckman, G. L. Bowlin and J. S. Wayne, *Tissue Engineering*, 2004, **10**, 1510–1517.
19 D. Li, J. T. McCann and Y. Xia, *Small*, 2005, **1**, 83–86.
20 B. Dong, O. Arnoult, M. E. Smith and G. E. Wnek, *Macromol. Rapid Commun.*, 2009, **30**, 539–542.
21 W. J. Li, C. T. Laurencin, E. J. Caterson, R. S. Tuan and F. K. Ko, *J. Biomed. Mater. Res.*, 2002, **60**, 613–621.
22 J. M. Deitzel, J. Kleinmeyer, D. Harris and N. C. Beck Tan, *Polymer*, 2001, **42**, 261–272.
23 K. H. Lee, H. Y. Kim, M. S. Khil, Y. M. Ra and D. R. Lee, *Polymer*, 2003, **44**, 1287–1294.
24 J. Xie, X. Li and Y. Xia, *Macromol. Rapid Commun.*, 2008, **29**, 1775–1792.
25 W. J. Li, K. G. Danielson, P. G. Alexander and R. S. Tuan, *J. Biomed. Mater. Res.*, 2003, **67a**, 1105–1114.
26 J. E. Sanders, D. V. Cassisi, T. Neumann, S. L. Golledge, S. G. Zachariah, B. D. Ratner and S. D. Bale, *J. Biomed. Mater. Res.*, 2003, **65a**, 462–467.
27 J. E. Sanders, C. E. Stiles and C. L. Hayes, *J. Biomed. Mater. Res.*, 2000, **52**, 231–237.
28 Z. Yin, X. Chen, J. L. Chen, W. L. Shen, T. M. Hieu Nguyen, L. Gao and H. W. Ouyang, *Biomaterials*, 31, pp. 2163–2175.
29 N. L. Nerurkar, B. M. Baker, C. Y. Chen, D. M. Elliott and R. L. Mauck, *Conf. Proc. IEEE Eng. Med. Biol. Soc.*, 2006, **1**, 787–790.
30 N. L. Nerurkar, D. M. Elliott and R. L. Mauck, *J. Orthop. Res.*, 2007, **25**, 1018–1028.
31 G. H. Kim, *Biomed. Mater.*, 2008, **3**, 25010.
32 H. Cao, K. Mchugh, S. Y. Chew and J. M. Anderson, *Journal of Biomedical Materials Research Part A*, 2010, **93A**, 1151–1159.
33 C. Hwang, Y. Park, J. Park, K. Lee, K. Sun, A. Khademhosseini and S. Lee, *Biomed. Microdevices*, 2009, **11**, 739–746.
34 F. T. Moutos, L. E. Freed and F. Guilak, *Nat. Mater.*, 2007, **6**, 162–167.
35 B. M. Baker, A. S. Nathan, G. R. Huffman and R. L. Mauck, *Osteoarthritis Cartilage*, 2009, **17**, 336–345.
36 L. S. Carnell, E. J. Siochi, N. M. Holloway, R. M. Stephens, C. Rhim, L. E. Niklason and R. L. Clark, *Macromolecules*, 2008, **41**, 5345–5349.
37 N. L. Nerurkar, B. M. Baker, S. Sen, E. E. Wible, D. M. Elliott and R. L. Mauck, *Nat. Mater.*, 2009, **8**, 986–992.
38 D. Li, G. Ouyang, J. T. McCann and Y. Xia, *Nano Lett.*, 2005, **5**, 913–916.
39 D. Li, Y. Wang and Y. Xia, *Nano Lett.*, 2003, **3**, 1167–1171.
40 D. Li, Y. Wang and Y. Xia, *Adv. Mater.*, 2004, **16**, 361–366.
41 C. Ayres, G. L. Bowlin, S. C. Henderson, L. Taylor, J. Shultz, J. Alexander, T. A. Telemeco and D. G. Simpson, *Biomaterials*, 2006, **27**, 5524–5534.
42 C. E. Ayres, G. L. Bowlin, R. Pizinger, L. T. Taylor, C. A. Keen and D. G. Simpson, *Acta Biomater.*, 2007, **3**, 651–661.
43 C. E. Ayres, B. S. Jha, H. Meredith, J. R. Bowman, G. L. Bowlin, S. C. Henderson and D. G. Simpson, *J. Biomater. Sci., Polym. Ed.*, 2008, **19**, 603–621.
44 F. Guilak, K. E. Lott, H. A. Awad, Q. Cao, K. C. Hicok, B. Fermor and J. M. Gimble, *J. Cell. Physiol.*, 2006, **206**, 229–237.
45 B. T. Estes, A. W. Wu and F. Guilak, *Arthritis Rheum.*, 2006, **54**, 1222–1232.
46 C.-Y. Huang, A. Stankiewicz, G. A. Ateshian, E. L. Flatlow, L. U. Bigliani and V. C. Mow, *Transactions of the Orthopaedic Research Society*, 1999, **24**, 95.
47 A. Verteramo and B. B. Seedhorn, *Biorheology*, 2004, **41**, 203–213.

